Unconventional quantum vortex matter state hosts quantum oscillations in the underdoped high-temperature cuprate superconductors

Yu-Te Hsu[a,1], Máté Hartstein[a], Alexander J. Davies[a], Alexander J. Hickey[a], Mun K. Chan[b], Juan Porras[c], Toshinao Loew[c], Sofia V. Taylor[a], Hsu Liu[a], Alexander G. Eaton[a], Matthieu Le Tacon[c,d], Huakun Zuo[e], Jinhua Wang[e], Zengwei Zhu[e], Gilbert G. Lonzarich[a], Bernhard Keimer[c], Neil Harrison[b,2], and Suchitra E. Sebastian[a,2]

[a]Cavendish Laboratory, Cambridge University, Cambridge CB3 0HE, United Kingdom; [b]Pulsed Field Facility, Los Alamos National Laboratory, Los Alamos, NM 87545; [c]Department of Solid State Spectroscopy, Max Planck Institute for Solid State Research, D-70569 Stuttgart, Germany; [d]Institute for Quantum Materials and Technology, Karlsruhe Institute of Technology, 1D-76344 Eggenstein-Leopoldshafen, Germany; and [e]National High Magnetic Field Center, School of Physics, Huazhong University of Science and Technology, Wuhan 430074, China

Edited by J. C. Séamus Davis, University College Cork, Cork, Ireland, and approved December 31, 2020 (received for review October 9, 2020)

A central question in the underdoped cuprates pertains to the nature of the pseudogap ground state. A conventional metallic ground state of the pseudogap region has been argued to host quantum oscillations upon destruction of the superconducting order parameter by modest magnetic fields. Here, we use low applied measurement currents and millikelvin temperatures on ultrapure single crystals of underdoped $YBa_2Cu_3O_{6+x}$ to unearth an unconventional quantum vortex matter ground state characterized by vanishing electrical resistivity, magnetic hysteresis, and nonohmic electrical transport characteristics beyond the highest laboratory-accessible static fields. A model of the pseudogap ground state is now required to explain quantum oscillations that are hosted by the bulk quantum vortex matter state without experiencing sizable additional damping in the presence of a large maximum superconducting gap; possibilities include a pair density wave.

high-T_c superconductivity | quantum vortex matter | cuprate pseudogap | quantum oscillations | high magnetic fields

Previous electrical transport measurements in underdoped $YBa_2Cu_3O_{6+x}$ (1) reported the occurrence of quantum oscillations above modest magnetic fields ≈22 T in a conventional metallic pseudogap ground state characterized by finite electrical resistivity, in which superconductivity is destroyed. Here, we access the ground state of a generation of pristine single crystals of underdoped $YBa_2Cu_3O_{6+x}$ (hole-doping concentration $p = 0.108 - 0.132$) up to the highest accessible static magnetic field of 45 T and down to 40 mK in the limit of low applied measurement current density ($j \to 0$). We find instead the persistence of vanishing electrical resistivity characteristic of magnetic field-resilient superconductivity beyond the highest accessible static magnetic field of 45 T.

In this work, we measure pristine single crystals of underdoped $YBa_2Cu_3O_{6+x}$ ($YBCO_{6+x}$) characterized by prominent quantum oscillations with a significantly lower Dingle (impurity-damping) factor than the previous generation of single crystals (2) (*SI Appendix*, Fig. S1). We access the longitudinal voltage in the ground state by applying a range of applied measurement current densities j down to low values of ≈0.01 $\mathrm{Acm^{-2}}$, three orders of magnitude lower than previously used values of ≈10 $\mathrm{Acm^{-2}}$. Fig. 1 *A*–*H* shows the effective resistivity [$\rho_{xx} = V_{xx}/(jl)$ where l is the distance between the voltage leads both in the case of ohmic and nonohmic transport characteristics] as a function of magnetic field and temperature. For sufficiently low applied measurement currents and temperatures, we find vanishing electrical resistivity that persists beyond the highest accessible static magnetic field of 45 T (Fig. 1 *A*–*H*). A steeply rising phase boundary of the resistive magnetic field scale up to which vanishing electrical resistivity persists in the limit of low applied measurement current [i.e., $\mu_0 H_r(j \to 0)$] as a function of temperature is shown in Fig. 2. A similarly sharply rising resistive magnetic field that shows no sign of saturation down to temperatures $\leq 0.001\,T_c(0)$ was reported by Mackenzie et al. (3) in pristine single crystals of $Tl_2Ba_2CuO_{6+\delta}$ (*SI Appendix*, Fig. S2), which also exhibits quantum oscillations (4).

The low values of critical current as a function of $\mu_0 H$ and T that we find to characterize high magnetic field-resilient superconductivity in high-purity single crystals of underdoped $YBa_2Cu_3O_{6+x}$ is consistent with a low density of pinning centers. Evidence of bulk superconductivity in the ground state is further revealed by magnetic hysteresis due to bulk vortex pinning in magnetic torque. We find good agreement between the resistive magnetic field in the limit of low applied measurement current [i.e., $\mu_0 H_r(j \to 0)$] and the high-magnetic field scale up to which hysteresis from bulk vortex pinning persists in the magnetic torque [i.e., the irreversibility field $\mu_0 H_{irr} = \mu_0 H_{irr}(\theta)\cos\theta$, where θ is the angle between the applied magnetic field and the crystalline c axis], up to the highest accessible static magnetic fields of 45 T as expected for bulk superconductivity (*Materials and Methods*, Fig. 2*A*, and *SI Appendix*, Figs. S3–S5) (5–8). Single crystals of the same doping from different batches and grown by different groups show similarly high irreversible magnetic fields

Significance

Modest magnetic fields above ≈22 T in the underdoped cuprates were argued to destroy superconductivity and reveal a conventional metallic pseudogap ground state that hosts quantum oscillations. We perform high-magnetic field electrical resistivity and magnetic torque measurements using low temperatures and small applied measurement currents to reveal instead an unconventional quantum vortex matter ground state that persists beyond the highest static magnetic fields. An alternative model is required to explain the coexistence of quantum oscillations with a robust *d*-wave superconducting gap in the newly uncovered quantum vortex matter ground state.

Author contributions: B.K., N.H., and S.E.S. designed research; Y.-T.H., M.H., A.J.D., A.J.H., M.K.C., J.P., T.L., S.V.T., H.L., A.G.E., M.L.T., H.Z., J.W., Z.Z., N.H., and S.E.S. performed research; Y.-T.H., M.H., A.J.D., A.J.H., G.G.L., N.H., and S.E.S. analyzed data; and N.H. and S.E.S. wrote the paper with input from all authors.

The authors declare no competing interest.

This article is a PNAS Direct Submission.

See online for related content such as Commentaries.

[1]Present addresses: High Field Magnet Laboratory and Institute for Molecules and Materials, Radboud University, 6525 ED Nijmegen, The Netherlands.

[2]To whom correspondence may be addressed. Email: suchitra@phy.cam.ac.uk or nharrison@lanl.gov.

This article contains supporting information online at https://www.pnas.org/lookup/suppl/doi:10.1073/pnas.2021216118/-/DCSupplemental.

Published February 9, 2021.

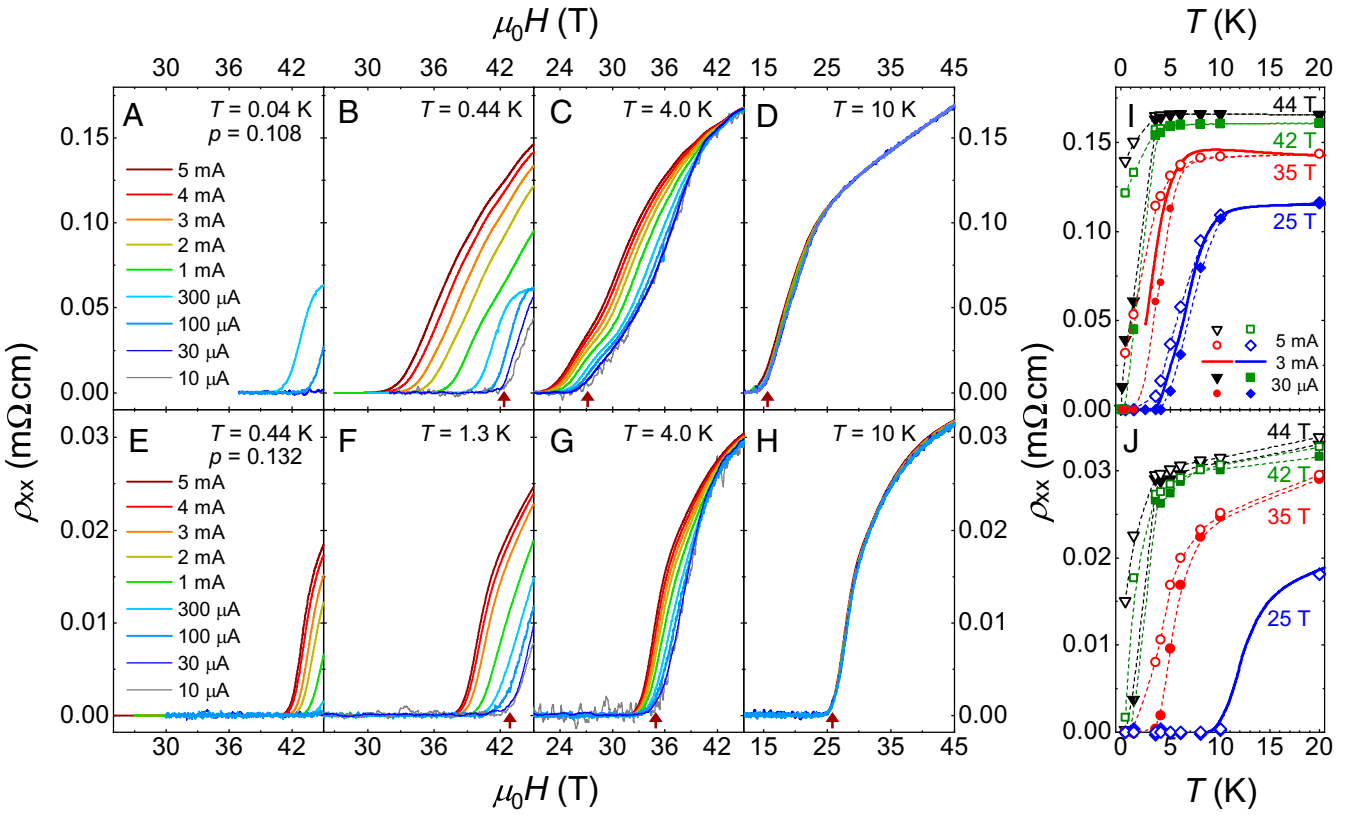

Fig. 1. Onset of finite electrical resistivity as a function of magnetic field for different applied measurement currents. (*A*–*H*) In-plane electrical resistivity ρ_{xx} of $YBa_2Cu_3O_{6+x}$ measured on sweeping the magnetic field ($\mu_0\mathbf{H} \parallel \hat{c}$) at different temperatures T, hole dopings p, and applied measurement currents I as indicated. Here, $\rho_{xx} = V_{xx}/(jl)$ is an effective resistivity in the nonohmic regime. Brown arrows indicate the resistive magnetic field ($\mu_0 H_r$) above which the electrical resistivity becomes finite in the limit of low applied measurement current [$\mu_0 H_r(j \to 0)$]. I= 1 mA corresponds for our samples to a current density of $j \approx 5$ Acm^{-2} assuming a limit of uniform current distribution. Superconductivity characterized by vanishing electrical resistivity in the $j \to 0$ limit is revealed to persist up to the highest accessible magnetic fields. At the lowest temperature of 40 mK, currents higher than 300 μA are expected to lead to self-heating effects, and hence, only measurements with applied currents below 100 μA are shown. (*I* and *J*) In-plane electrical resistivity ρ_{xx} transition into the superconducting state characterized by vanishing electrical resistivity in the $j \to 0$ limit shown at different values of magnetic field (symbols show pulsed field data, dashed lines connecting symbols are guides to the eye, and solid lines show continuous field data). Width of the superconducting transition is similarly narrow to that observed at zero magnetic fields. Symbols in *I* also apply to *J*.

in agreement with the high resistive magnetic fields we access in this work (*SI Appendix*, Fig. S3).

We provide further evidence that argues against an origin of magnetic field-resilient superconductivity in the ground state of underdoped $YBa_2Cu_3O_{6+x}$ high critical temperature doping inclusions. Superconducting homogeneity is indicated by the narrow superconducting transition in the electrical resistivity as a function of temperature in high magnetic fields (Fig. 1 *I* and *J*). Further support for superconducting homogeneity is provided by the sharpness of the transition in the magnetic susceptibility (χ) in very small magnetic fields (*SI Appendix*, Figs. S6 and S7), from which we infer a minimal volume fraction of any regions of the sample with a value of T_c greater than the mean T_c (defined by the step in χ). The observation of low critical temperatures at high magnetic fields further argues against the inclusions of higher dopings as responsible for the persistence of superconductivity up to high magnetic fields. The systematic doping evolution of the high-field superconducting region, which reaches higher critical temperatures with increasing doping, also supports the intrinsic bulk character of the high magnetic field-resilient superconductivity (Fig. 2).

In order to discern the nature of the high-field superconducting ground state, we perform a study of the voltage–current characteristics, signatures of which are used to characterize regimes of superconducting vortex physics (9). We find a striking and systematic nonohmic voltage–current dependence at high magnetic fields and low temperatures (Fig. 3 *A*–*E*). Given that previous measurements in the vortex state were largely confined to low magnetic fields and high temperatures (9), we use a new model of unconventional quantum vortex matter developed to treat the high-magnetic field region to compare with our measurements in the high-magnetic field–low-temperature region of underdoped $YBa_2Cu_3O_{6+x}$ (10). We find that the measured nonohmic voltage–current dependence can be well captured by a model of quantum vortex matter based on self-organization of vortices in a magnetic field (10, 11). We use the term "quantum vortex matter" to describe the vortex regime in high magnetic fields and low temperatures where quantum fluctuations are expected to be relevant (10), as opposed to the more conventional vortex regime at low magnetic fields and high temperatures (9). We extract a temperature scale (10) (T_{HFF}) associated with the melting of quantum vortex matter into a vortex liquid (Fig. 3*F*) for various magnetic fields and find that the quantum vortex matter–vortex liquid phase boundary agrees well with the extracted resistive magnetic field $\mu_0 H_r$, below which the voltage drops to a vanishingly small value for a range of temperatures (Fig. 2*A*). Our findings thus unearth a bulk quantum vortex matter ground state that persists up to at least 45 T and evolves to a vortex liquid with increasing temperature as shown in the phase diagrams (Fig. 2 and *SI Appendix*, Fig. S8; see Fig. 4*E*). A similar superconducting phase diagram driven by quantum fluctuations has been reported in two-dimensional materials families such as the organic superconductors (12), and may be similarly expected in the strongly

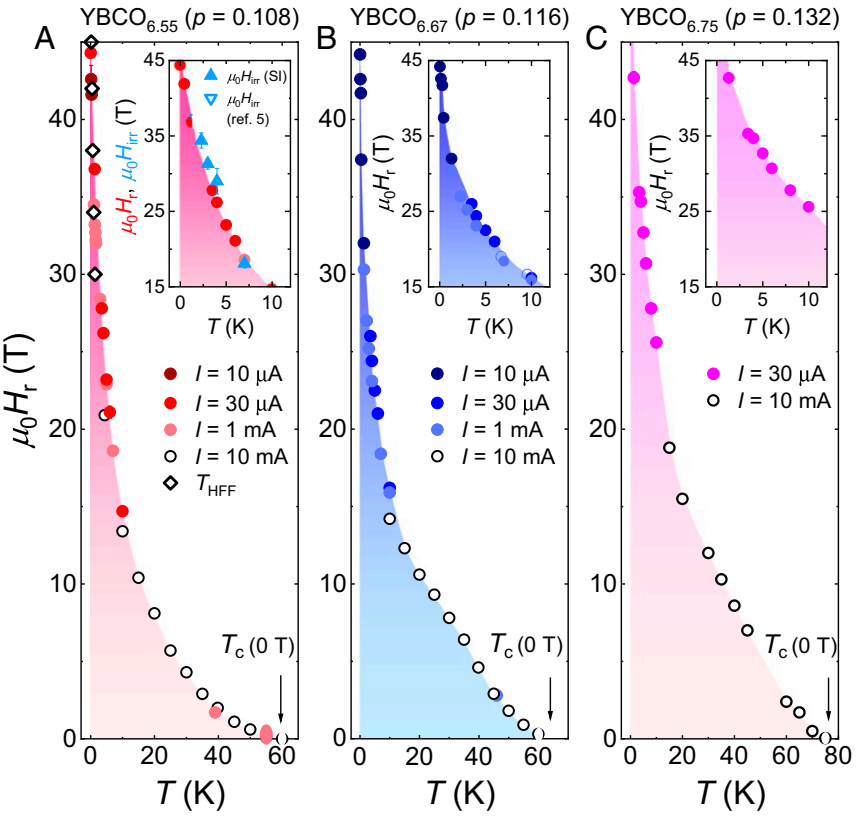

Fig. 2. Magnetic field-resilient superconductivity revealed at low temperatures and low applied measurement currents. Resistive magnetic field $\mu_0 H_r$ measured for $YBa_2Cu_3O_{6+x}$ ($YBCO_{6+x}$) at three hole dopings, (*A*) p = 0.108, (*B*) p = 0.116, and (*C*) p = 0.132, using static magnetic field scans at different fixed temperatures and currents I indicated by circles (here, a current of I= 1 mA corresponds to a current density $j \approx 5$ Acm^{-2}), obtained from Fig. 1. *A*–*C*, *Insets* show expanded views in the high-field low-temperature region. Magnetic field-resilient superconductivity is observed to persist up to the highest magnetic fields for low applied measurement currents. Similarly, nonsaturating values of resistive magnetic field down to the lowest temperatures were reported in $Tl_2Ba_2CuO_{6+\delta}$ (*SI Appendix*, Fig. S2) (3). The temperature scale associated with the melting of quantum vortex matter into a vortex liquid (T_{HFF}) is indicated by diamonds in *A*. The bulk character of superconductivity at high magnetic fields is indicated by the similar phase boundary obtained from magnetic torque measurements (*A*, *Inset*).

interacting quasitwo-dimensional cuprate superconductors. Similarly, non–BCS (Bardeen–Cooper–Schrieffer)-like magnetic field-resilient superconductivity with positive curvature of the resistive magnetic field was reported in high-purity single crystals of $Tl_2Ba_2CuO_{6+\delta}$ (3). An interplay of superconductivity and a density wave (13) has been further proposed to yield a steep magnetic field–temperature slope of the superconducting phase boundary, as observed in our experiments.

The finite resistivity previously accessed above a modest magnetic field scale ≈22 T in underdoped $YBa_2Cu_3O_{6+x}$ (1) can be attributed to the use in pulsed magnetic field experiments of applied measurement current densities three orders of magnitude higher than present measurements and even larger eddy current densities (*Materials and Methods*) at elevated temperatures (*SI Appendix*, Fig. S9), yielding vortex dissipation. Previous heat capacity measurements were performed at elevated temperatures and do not access low-enough temperatures to capture the unconventional quantum vortex matter regime (*SI Appendix*, Fig. S9) (14). Features in thermal conductivity previously interpreted as a signature of the upper critical magnetic field in $YBa_2Cu_3O_{6+x}$ (1) meanwhile differ from signatures of the upper critical magnetic field as observed in other type II superconductors (*SI Appendix*, Fig. S10), prompting its alternative interpretation as a density wave transition in $YBa_2Cu_3O_{6+x}$ (5).

The superconducting phase diagram in high-magnetic field–low-temperature space for the underdoped cuprates revealed by our present measurements is shown in Fig. 4*E* and *SI Appendix*, Fig. S11. We find the quantum vortex matter region characterized by vanishing electrical resistivity in the $j \to 0$ limit and nonohmic voltage–current characteristics (colored shading) to steeply rise at low temperatures, persisting beyond the highest laboratory-accessible static magnetic fields of 45 T. The newly uncovered high-magnetic field superconducting phase diagram supercedes previous proposals involving a finite electrical resistivity ground state (*SI Appendix*, Fig. S8 *A* and *B*). Previous proposals include a BCS-like type II superconducting phase diagram in which a Meissner superconducting state rapidly enters a conventional metallic region (1, 14) at high magnetic fields via a vortex solid (Shubnikov-phase) region (9) (*SI Appendix*, Figs. S8*A* and S12) and the alternative possibility of a vortex liquid ground state at high magnetic fields characterized by finite electrical resistivity (5, 15, 16) (*SI Appendix*, Fig. S8*B*).

We gain insight into the character of the quantum vortex matter ground state of the pseudogap by examining the quantum oscillations that are hosted in this region characterized by hysteretic magnetic torque (zero applied measurement current) evidencing vortex pinning (5, 6), vanishing electrical resistivity in the $j \to 0$ limit, and nonohmic electrical transport (Fig. 4 *A* and *B*). Quantum oscillations in the electrical resistivity also appear in the quantum vortex matter region, upon the application of sufficiently elevated currents for finite resistivity to be induced from vortex dissipation (Fig. 4*D*). We compare quantum oscillations in the superconducting region of underdoped $YBa_2Cu_3O_{6+x}$ with those observed in other type II superconductors including $NbSe_2$, V_3Si, Nb_3Sn, YNi_2B_2C, $LuNi_2B_2C$, $UPdAl_3$, URu_2Si_2, $CeCoIn_5$, $CeRu_2$, κ-(BEDT-TTF)$_2$Cu(NCS)$_2$, MgB_2, and others (17–19), for which theories have been developed of quantum oscillations in the mixed state (e.g., refs. 19 and 20). To estimate the extent of superconducting damping of quantum oscillations, we compare the ratio of the Landau-level spacing $\hbar\omega_c$ to the maximum superconducting gap Δ (here, $\omega_c = e\mu_0 H/m^*$ is the cyclotron frequency and m^* is the cyclotron effective mass) at magnetic fields where superconducting damping reduces the quantum oscillation amplitude (corrected for the Dingle damping factor) by a factor of two (21). In the case of underdoped $YBa_2Cu_3O_{6+x}$, we obtain an upper bound for this ratio at the lowest magnetic field value at which quantum oscillations are observed. A low value of $\hbar\omega_c/\Delta \lessapprox 0.06$ is estimated for underdoped $YBa_2Cu_3O_{6+x}$, taking the maximum superconducting gap at zero magnetic field $\Delta \approx 30$ meV from complementary measurements (22) (consistent with the high-magnetic field resilience of superconductivity), $m^* = 1.6\ m_e$ (m_e is the free electron mass) (23), and $\mu_0 H = 20$ T. This ratio in underdoped

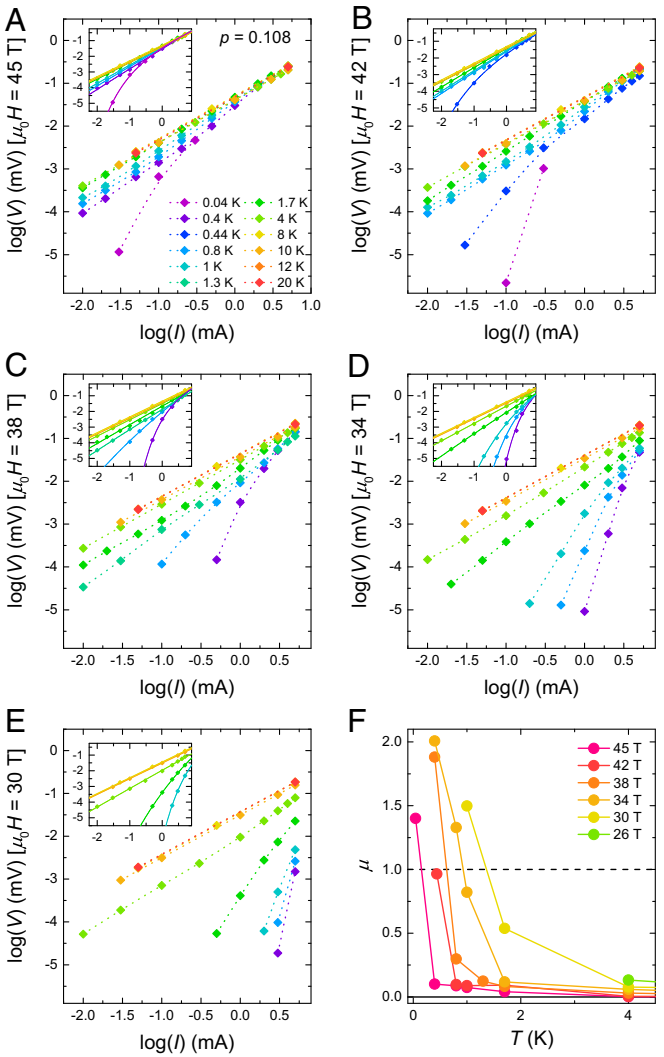

Fig. 3. Nonohmic voltage–current dependence at the highest magnetic fields and lowest temperatures. (*A–E*) In-plane longitudinal voltage measured for $YBa_2Cu_3O_{6+x}$ ($p = 0.108$) as a function of applied measurement current, at temperatures ranging from 20 K down to 0.04 K at different applied magnetic fields. Voltage values measured at the same temperature are connected by dashed lines. Solid lines in *Insets* in *A–E* correspond to fits based on a model of quantum vortex matter by Huse and coworkers (10), characterized by nonohmic current–voltage dependence described by $V \propto j \exp[-(j_T/j)^{\mu}]$, where j is the current density and j_T and μ are fitting parameters. (*F*) The exponent μ as a function of temperature, with T_{HFF} defined as the temperature when $\mu = 1$.

$YBa_2Cu_3O_{6+x}$ is an order of magnitude smaller than the ratio $\hbar\omega_c/\Delta \approx 0.5$ for conventional type II superconductors including $NbSe_2$, V_3Si, Nb_3Sn, YNi_2B_2C, $LuNi_2B_2C$, $CeRu_2$, and MgB_2 (details are in *SI Appendix*, Table S1). Quantum oscillations thus persist in the presence of a large maximum superconducting gap, displaying minimal superconducting damping in the case of underdoped $YBa_2Cu_3O_{6+x}$, unlike conventional type II superconductors. Similarly low ratios of $\hbar\omega_c/\Delta$ as underdoped $YBa_2Cu_3O_{6+x}$ are found in unconventional type II superconductors such as URu_2Si_2 ($\hbar\omega_c/\Delta \approx 0.08$ for Δ_{ab} and ≈ 0.04 for Δ_c), κ-(BEDT-TTF)$_2$Cu(NCS)$_2$ ($\hbar\omega_c/\Delta \approx 0.05$), and UPd_2Al_3 ($\hbar\omega_c/\Delta \approx 0.006$ for Δ_{ab} and ≈ 0.3 for Δ_c) (details are in *SI Appendix*, Table S1).

Models of quantum oscillations in the presence of a spatially uniform superconducting gap associate a low ratio of $\hbar\omega_c/\Delta$ in unconventional type II superconductors with an anisotropic d-wave superconducting gap, compared with a higher ratio of $\hbar\omega_c/\Delta$ in the case of conventional type II superconductors characterized by an isotropic superconducting gap (24–28). Inspection of quantum oscillations in the quantum vortex matter state of underdoped $YBa_2Cu_3O_{6+x}$, however, reveals distinguishing characteristics that are challenging to reconcile with models of spatially uniform superconductivity. First, in models of spatially uniform superconductivity, whether characterized by isotropic superconducting gapping over the full Fermi surface or d-wave superconducting gapping over the full Fermi surface except at a gapless nodal point, the quantum oscillation amplitude is expected to exhibit a reduced temperature variation at low temperatures due to the vanishing of in-gap states (9, 19–21, 24, 29). In contrast, the quantum oscillation amplitude increases at low temperatures in underdoped $YBa_2Cu_3O_{6+x}$, consistent with the Lifshitz–Kosevich form (30) even within the quantum vortex matter state, signaling Fermi–Dirac statistics of low-energy excitations within the gap (Fig. 4*C*). Second, models of spatially uniform superconductivity are expected to yield increased damping both as the system transitions from the "normal" metallic regime in which the superconducting order parameter is destroyed to the vortex liquid regime in which vortices are mobile and as the system further transitions to the quantum vortex matter regime in which vortices are collectively pinned (Fig. 4*E*). In our present experiments, we access quantum oscillations as the system transitions from a mobile vortex liquid state to the pinned quantum vortex matter state (Fig. 4 *B* and *E*). In contrast to the expectation from models of spatially uniform superconductivity, no discernible additional damping beyond that in the usual Lifshitz–Kosevich description is observed as the quantum oscillations evolve from the vortex liquid regime to the quantum vortex matter regime (Fig. 4 *B* and *C* and *SI Appendix*, Figs. S13 and S14). These properties of the quantum oscillations we observe in the quantum vortex matter regime reveal the coexistence of finite gapless excitations with a large maximum superconducting gap.

The observed coexistence can potentially be explained by nonuniform models of superconductivity that are spatially modulated at a finite wave vector, such as the pair density wave (PDW) recently reported in experiments such as scanning–tunneling microscopy (31–44). Unlike models of spatially uniform superconductivity that are characterized by nodal points (9, 19–21, 24, 29), models of finite wave vector superconductivity result in "nesting" over only a portion of the Fermi surface and consequently, yield a partially gapped Fermi surface and lines of gapless excitations (31). PDW models display a nodal–antinodal dichotomy in which the antinodes are gapped by a large maximum superconducting gap, while gapless "Fermi arcs" occur near the nodes (31, 32, 34, 37). The reconstruction of the gapless nodal Fermi arcs in PDW models yields a sharply defined nodal Fermi pocket, providing a possible explanation for our observation of quantum oscillations hosted in a quantum vortex matter ground state, which are largely undamped by the large maximum superconducting gap. Alternatively, a nodal Fermi pocket has been modeled to arise from Fermi surface reconstruction by biaxial charge density wave order (45). Our observations potentially point to quantum oscillations in the quantum vortex matter regime due to the interplay of superconductivity and biaxial charge density wave order.

Any model of quantum oscillations in the unconventional quantum vortex matter ground state of the pseudogap region must also explain features such as the isolated nodal Fermi pocket found by complementary observations of forward–sawtooth form quantum oscillations (2), low measured value of linear specific heat capacity in high magnetic fields (46), the high magnetic field saturation of quantities such as the specific heat capacity (1), and the spin susceptibility from the Knight shift (47). An open question pertains to the extent to which vortex physics persists over the broader doping, temperature, and magnetic field range of the pseudogap region of the underdoped cuprate phase diagram (31, 34, 48).

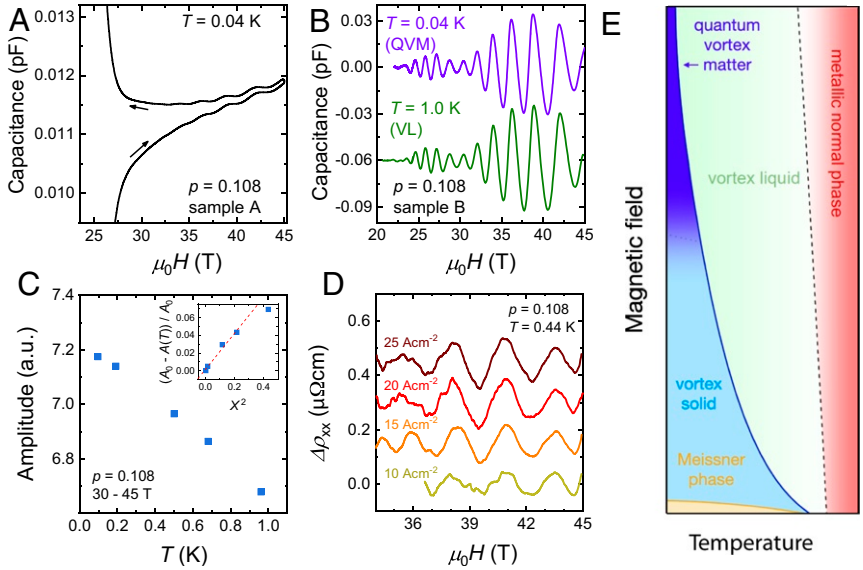

Fig. 4. Quantum oscillations coexisting with the vortex matter phase and the magnetic field–temperature phase diagram for $YBa_2Cu_3O_{6+x}$. (*A*) Quantum oscillations coexist with hysteresis in magnetic torque (zero applied measurement current, $\theta = 9°$) from vortex pinning extending up to the irreversibility field $\mu_0 H_{irr}$ beyond 45 T, coincident with the vanishing electrical resistivity region that also extends beyond 45 T at $T = 0.04$ K (*SI Appendix*, Fig. S3). (*B*) Quantum oscillations in the quantum vortex matter (QVM) regime at the lowest temperature $T = 0.04$ K are seen to be of similar size to quantum oscillations in the finite electrical resistivity vortex liquid (VL) region at elevated temperature $T = 1.0$ K (*SI Appendix*, Fig. S13). (*C*) Lifshitz–Kosevich (LK) temperature dependence of the quantum oscillation amplitude at the lowest measured temperatures. *Inset* shows that the growth of quantum oscillation amplitude continues to the lowest measured temperatures, as brought out by a low-temperature expansion (*Materials and Methods*). $A(T)$ is the quantum oscillation amplitude at temperature T, A_0 is the amplitude at the lowest measured temperature, and $X = 2\pi^2 k_B T m^*/e\hbar\mu_0 H$ is the temperature damping coefficient in the LK formula (50). (*D*) Shubnikov–de Haas oscillations after background subtraction in the QVM regime upon applying elevated current densities to induce vortex dissipation. Here, $\rho_{xx} = V_{xx}/(jl)$ is an effective resistivity in the nonohmic regime. (*E*) Superconducting phase diagram in which high magnetic field-resilient QVM ground state is revealed in the present measurements, melting to a VL with elevated temperature.

Materials and Methods

Sample Preparation for Transport Measurements. The electrical transport is measured on pristine detwinned oxygen-ordered single crystals of $YBa_2Cu_3O_{6+x}$ grown by the flux technique. Samples with typical dimensions of (0.8 to 1.5) × (0.5 to 1.0) × (0.03 to 0.08) mm were selected for the electrical transport measurements. Gold pads of standard six-contact geometry were deposited onto the top surface with 160-nm thickness and to the sides with 80-nm thickness using thermal evaporation methods. Top and side views of a typical transport sample are shown in *SI Appendix*, Fig. S1. Samples with gold pads were annealed at temperatures above 500 °C with flow of high-purity oxygen (>99.9999%) to set the oxygen content x and meanwhile, allow the gold pads to diffuse into the bulk of the crystal. All measurements in this work were performed with current flowing along the $\hat{a}$ axis, with crystals detwinned under uniaxial stress of 100 MPa at 250 °C. Cu–O chain superstructures were formed in samples under vacuum conditions of below 3×10^{-2} mbar. Samples with current contact resistances of ≈0.5 Ω, made using gold wires attached with DuPont 4929N, were used for high-field measurements. *SI Appendix*, Fig. S2 shows the superconducting transitions in the susceptibility for the measured samples, with transition widths similar to previous reports. Hole doping p is inferred from the critical temperature T_c (49), defined as the midpoint of the superconducting transition.

Evidence for Bulk Superconductivity. An important question concerning the observation of superconductivity that persists up to high magnetic fields is whether the superconductivity is of bulk character. Fig. 1 *I* and *J* presents measurements of the electrical resistivity vs. temperature for $p = 0.108$, 0.132. The narrow absolute width of the superconducting transition in electrical resistivity at high magnetic fields indicates no significant increase in inhomogeneity of the superconducting state in strong magnetic fields when T_c is suppressed. Furthermore, an inclusion of a small superconducting volume fraction of a higher doping, were it to exist, would manifest in magnetic susceptibility measurements, which is not observed, as shown in *SI Appendix*, Fig. S3.

The observation of significant vortex pinning in the magnetic torque (i.e., hysteresis in Fig. 4*A* and *SI Appendix*, Fig. S4*C*) accompanying vanishing electrical resistivity in the $j \to 0$ limit below the superconducting transition indicates a bulk superconducting state. No such sharp transition or hysteretic signature in the bulk magnetic torque is expected to occur for surface or filamentary superconducting states (8), which furthermore, typically exhibit small finite electrical resistivity rather than the vanishing electrical resistivity that is observed. The above findings and the systematic nature and sample independence of our results point to the intrinsic, bulk character of the magnetic field-resilient superconducting state in the pseudogap ground state characterized by low critical temperature and low critical current that we find to be persistent beyond the highest-accessible static magnetic fields of 45 T.

Low-Temperature Growth of Quantum Oscillation Amplitude Compared with Lifshitz–Kosevich Expansion. The Fermi–Dirac distribution yields a temperature-dependent quantum oscillation amplitude in the Lifshitz–Kosevich form (50). This low-temperature growth of quantum oscillation amplitude is given by

$$R_T = \frac{X}{\sinh X},$$

with $X = 2\pi^2 k_B T m^*/e\hbar\mu_0 H$, where k_B is Boltzmann's constant, T is temperature, m^* is the quasiparticle effective mass, e is the electron charge, and $\hbar$ is the reduced Planck constant (50). For small T, a series expansion of the temperature dependence term yields

$$R_T \approx 1 - \frac{X^2}{6} + O\left(X^4\right).$$

For small T, therefore, the quantum oscillation amplitude linearly increases with decreasing X^2 approaching the $T \to 0$ limit. The low-temperature growth in quantum oscillation amplitude is captured by the relative change of quantum oscillation amplitude at a finite temperature $A(T)$ with respect to the amplitude at the lowest measured temperature A_0, given by

$$1 - \frac{A(T)}{A_0} = \frac{A_0 - A(T)}{A_0} = \frac{X^2}{6}.$$

A plot of $(A_0 - A(T))/A_0$ against X^2 would therefore yield a straight line with a gradient equal to 1/6 at low temperatures for low-energy excitations within the gap. In contrast, in the absence of low-energy excitations,

gapped quantum oscillation models would yield a much reduced change in amplitude as a function of X^2 at low temperatures well below the gap temperature scale (24). Fig. 4 *C*, *Inset* shows the growth in quantum oscillation amplitude plotted against X^2 with a quasiparticle effective mass $m^*/m_e = 1.676$ (51). The rapid low-temperature growth of the quantum oscillation amplitude yields a linear slope of 0.20 (2) at low temperatures, in notable contrast to the expectation of little to no growth in the case of gapped quantum oscillations in the low-temperature limit. A full temperature dependence of the quantum oscillation amplitude up to a temperature of 18 K is shown in *SI Appendix*, Fig. S14.

Data Availability. All data are included in the manuscript and/or *SI Appendix*.

ACKNOWLEDGMENTS. Y.-T.H., M.H., A.J.D., A.J.H., S.V.T., H.L., and S.E.S. acknowledge support from the Royal Society; the Winton Program for the Physics of Sustainability; an Engineering and Physical Sciences Research Council (EPSRC) studentship; EPSRC Grants EP/R513180/1, EP/M506485/1, and EP/P024947/1; and the European Research Council under the European Union's Seventh Framework Program Grants 337425 and 772891. H.Z., J.W., and Z.Z. acknowledge support from National Key Research and Development Program of China Grant 2016YFA0401704. S.E.S. acknowledges support from the Leverhulme Trust by way of the award of a Philip Leverhulme Prize. Some of magnetic measurements were carried out using the Advanced Materials Characterization Suite in the University of Cambridge, funded by EPSRC Strategic Equipment Grant EP/M000524/1. A portion of this work was performed at the National High Magnetic Field Laboratory, which is supported by NSF Cooperative Agreement DMR-1157490, the State of Florida, and the Department of Energy. M.K.C. and N.H. acknowledge support from the Department of Energy BES project: "Science of 100 tesla." We thank S. A. Kivelson for suggesting the application of the vortex model of Huse et al. to our data. We are grateful for helpful discussions with colleagues including P. W. Anderson, L. Benfatto, J. Blatter, J. C. S. Davis, N. Doiron-Leyraud, M. Eisterer, E. M. Forgan, R. H. Friend, D. Geshkenbein, P. Kim, S. A. Kivelson, M. H. Julien, D. H. Lee, P. A. Lee, T. Maniv, D. R. Nelson, M. R. Norman, N. P. Ong, C. Pepin, M. Randeria, S. Sachdev, J. Schmalian, T. Senthil, L. Taillefer, C. M. Varma, and H. H. Wen. We are also grateful for experimental support at National High Magnetic Field Laboratory Tallahassee from J. Billings, E. S. Choi, B. L. Dalton, D. Freeman, L. J. Gordon, D. E. Graf, M. Hicks, S. A. Maier, T. P. Murphy, J.-H. Park, K. N. Piotrowski, and others. We thank S. Lacher and C. T. Lin for assistance with synthesis of high-quality single crystals.

1. C. Proust, L. Taillefer, The remarkable underlying ground states of cuprate superconductors. *Annu. Rev. Condensed Matter Phys.* **10**, 409–429 (2019).
2. M. Hartstein *et al.*, Hard antinodal gap revealed by quantum oscillations in the pseudogap regime of underdoped high-T_c superconductors. *Nat. Phys.* **16**, 841–847 (2020).
3. A. Mackenzie *et al.*, Resistive upper critical field of $Tl_2Ba_2CuO_6$ at low temperatures and high magnetic fields. *Phys. Rev. Lett.* **71**, 1238–1241 (1993).
4. P. Rourke *et al.*, A detailed de Haas–van Alphen effect study of the overdoped cuprate $Tl_2Ba_2CuO_{6+\delta}$. *New J. Phys.* **12**, 105009 (2010).
5. F. Yu *et al.*, Magnetic phase diagram of underdoped $YBa_2Cu_3O_y$ inferred from torque magnetization and thermal conductivity. *Proc. Natl. Acad. Sci. U.S.A.* **113**, 12667–12672 (2016).
6. S. E. Sebastian *et al.*, A multi-component Fermi surface in the vortex state of an underdoped high-T_c superconductor. *Nature* **454**, 200–203 (2008).
7. W. Druyvesteyn, D. Van Ooijen, T. Berben, Variation of the critical fields of superconducting lead with the residual resistivity. *Rev. Mod. Phys.* **36**, 58–61 (1964).
8. L. Lyard *et al.*, Anisotropy of the upper critical field and critical current in single crystal MgB_2. *Phys. Rev. B* **66**, 180502 (2002).
9. G. Blatter, V. B. Geshkenbein, "Vortex matter"in *The Physics of Superconductors*, K. H. Bennemann, J. B. Ketterson, Eds. (Springer, Berlin, Germany, 2003), pp. 725–936.
10. F. Fisher, S. Daniel, P. Matthew, D. A. Huse, Thermal fluctuations, quenched disorder, phase transitions, and transport in type-II superconductors. *Phys. Rev. B* **43**, 130–159 (1991).
11. D. A. Huse, Fisher, P. Matthew, D. S. Fisher, Are superconductors really superconducting? *Nature* **358**, 553–559 (1992).
12. T. Sasaki *et al.*, Low-temperature vortex liquid states induced by quantum fluctuations in the quasi-two-dimensional organic superconductor κ-$(BEDT\text{-}TTF)_2Cu(NCS)_2$. *Phys. Rev. B* **66**, 224513 (2002).
13. Y. Yu, S. A. Kivelson, Fragile superconductivity in the presence of weakly disordered charge density waves. *Phys. Rev. B* **99**, 144513 (2019).
14. C. Marcenat *et al.*, Calorimetric determination of the magnetic phase diagram of underdoped ortho II $YBa_2Cu_3O_{6.54}$ single crystals. *Nat. Commun.* **6**, 7927 (2015).
15. Y. Wang, L. Li, N. P. Ong, Nernst effect in high-T_c superconductors. *Phys. Rev. B* **73**, 024510 (2006).
16. L. Li *et al.*, Diamagnetism and Cooper pairing above T_c in cuprates. *Phys. Rev. B* **81**, 054510 (2010).
17. R. Corcoran *et al.*, De Haas-van Alphen effect in the superconducting state. *Phys. B Condens. Matter* **206**, 534–541 (1995).
18. Y. Onuki, R. Settai, de Haas–van Alphen effect in strongly correlated electron systems. *Phys. B Condens. Matter* **300**, 61–77 (2001).
19. T. Maniv, V. Zhuravlev, I. Vagner, P. Wyder, Vortex states and quantum magnetic oscillations in conventional type-II superconductors. *Rev. Mod. Phys.* **73**, 867–911 (2001).
20. K. Yasui, T. Kita, Theory of the de Haas–van Alphen effect in type-II superconductors. *Phys. Rev. B* **66**, 184516 (2002).
21. T. Janssen *et al.*, Quantitative investigation of the de Haas-van Alphen effect in the superconducting state. *Phys. Rev. B* **57**, 11698 (1998).
22. S. Hüfner, M. Hossain, A. Damascelli, G. Sawatzky, Two gaps make a high-temperature superconductor? *Rep. Prog. Phys.* **71**, 062501 (2008).
23. S. E. Sebastian *et al.*, Quantum oscillations from nodal bilayer magnetic breakdown in the underdoped high temperature superconductor $YBa_2Cu_3O_{6+x}$. *Phys. Rev. Lett.* **108**, 196403 (2012).
24. K. Miyake, de Haas-van Alphen oscillations in superconducting states as a probe of gap anisotropy. *Phys. B Condens. Matter* **186**, 115–117 (1993).
25. A. Melikyan, O. Vafek, Quantum oscillations in the mixed state of d-wave superconductors. *Phys. Rev. B* **78**, 020502 (2008).
26. C. Varma, Magneto-oscillations in underdoped cuprates. *Phys. Rev. B* **79**, 085110 (2009).
27. M. Franz, Z. Tešanović, Self-consistent electronic structure of a $d_{x^2-y^2}$ and a $d_{x^2-y^2} + id_{xy}$ vortex. *Phys. Rev. Lett.* **80**, 4763 (1998).
28. M. R. Norman, A. MacDonald, H. Akera, Magnetic oscillations and quasiparticle band structure in the mixed state of type-II superconductors. *Phys. Rev. B* **51**, 5927–5942 (19955).
29. S. Banerjee, S. Zhang, M. Randeria, Theory of quantum oscillations in the vortex state of high-T_c superconductors. *Nat. Commun.* **4**, 1700 (2013).
30. S. E. Sebastian *et al.*, Fermi-liquid behavior in an underdoped high-T_c superconductor. *Phys. Rev. B* **81**:140505(R) (2010).
31. D. F. Agterberg *et al.*, The physics of pair density waves: Cuprate superconductors and beyond. *Annu. Rev. Condensed Matter Phys.* **11**, 231–270 (2020).
32. Z. Dai, Y. H. Zhang, T. Senthil, P. A. Lee, Pair-density waves, charge-density waves, and vortices in high-T_c cuprates. *Phys. Rev. B* **97**, 174511 (2018).
33. Z. Dai, T. Senthil, P. A. Lee, Modeling the pseudogap metallic state in cuprates: Quantum disordered pair density wave. *Phys. Rev. B* **101**, 064502 (2020).
34. E. Berg, E. Fradkin, K. A. Kivelson, J. M. Tranquanda, Striped superconductors: How spin, charge and superconducting orders intertwine in the cuprates. *New J. Phys.* **11**, 115004 (2009).
35. M. Norman, J. S. Davis, Quantum oscillations in a biaxial pair density wave state. *Proc. Natl. Acad. Sci. U.S.A.* **115**, 5389–5391 (2018).
36. S. D. Edkins *et al.*, Magnetic field–induced pair density wave state in the cuprate vortex halo. *Science* **364**, 976–980 (2019).
37. S. Baruch, D. Orgad, Spectral signatures of modulated *d*-wave superconductors. *Phys. Rev. B* **77**, 174502 (2008).
38. Z. Du *et al.*, Imaging the energy gap modulations of the cuprate pair-density-wave state. *Nature* **580**, 65–70 (2020).
39. D. Chakraborty *et al.*, Fractionalized pair density wave in the pseudogap phase of cuprate superconductors. *Phys. Rev. B* **100**, 224511 (2019).
40. P. Choubey *et al.*, Atomic-scale electronic structure of the cuprate pair density wave state coexisting with superconductivity. *Proc. Natl. Acad. Sci. U.S.A.* **117**, 14805–14811 (2020).
41. Y. Wang *et al.*, Pair density waves in superconducting vortex halos. *Phys. Rev. B* **97**, 174510 (2018).
42. M. Zelli, C. Kallin, A. J. Berlinsky, Quantum oscillations in a π-striped superconductor. *Phys. Rev. B* **86**, 104507 (2012).
43. M. H. Hamidian *et al.*, Detection of a Cooper-pair density wave in $Bi_2Sr_2CaCu_2O_{8+x}$. *Nature* **532**, 343–347 (2016).
44. H. D. Chen, O. Vafek, A. Yazdani, S. C. Zhang, Pair density wave in the pseudogap state of high temperature superconductors. *Phys. Rev. Lett.* **93**, 187002 (2004).
45. S. E. Sebastian, N. Harrison, G. Lonzarich, Towards resolution of the Fermi surface in underdoped high-T_c superconductors. *Rep. Prog. Phys.* **75**, 102501 (2012).
46. S. C. Riggs *et al.*, Heat capacity through the magnetic-field-induced resistive transition in an underdoped high-temperature superconductor. *Nat. Phys.* **7**, 332–335 (2011).
47. R. Zhou *et al.*, Spin susceptibility of charge-ordered $YBa_2Cu_3O_y$ across the upper critical field. *Proc. Natl. Acad. Sci. U.S.A.* **114**, 13148–13153 (2017).
48. P. A. Lee, Amperean pairing and the pseudogap phase of cuprate superconductors. *Phys. Rev. X* **4**, 031017 (2014).
49. R. Liang, D. A. Bonn, W. N. Hardy, Evaluation of CuO_2 plane hole doping in $YBa_2Cu_3O_{6+x}$ singly crystals. *Phys. Rev. B* **73**, 180505(R) (2006).
50. D. Shoenberg, *Magnetic Oscillations in Metals* (Cambridge University Press, Cambridge, United Kingdom, 1984).
51. S. E. Sebastian *et al.* Fermi-liquid behavior in an underdoped high-T_c superconductor. *Phys. Rev. B* **81**, 140505 (2010).